

Supporting Information

Unveiling enhanced mechanism of alkaline hydrogen evolution kinetics on molybdenum-cobalt sulfides for efficient anion exchange membrane water electrolyzer

Jingbin Huang,^a Bin Hu,^a Yunlin Li,^a Jie Zhu,^{*b} Jing Jiang,^a Han Zhao,^a Jingxian Zhou,^a Lin Jin^{*a} and Renbing Wu^{*c}

^aInternational Joint Research Laboratory for Biomedical Nanomaterials of Henan, Henan Key Laboratory of Rare Earth Functional Materials, College of Chemistry & Chemical Engineering, Zhoukou Normal University, Zhoukou, 466001, P. R. China.

^bSchool of Materials Science and Engineering, Guilin University of Technology, Guilin, 541000, P. R. China.

^cDepartment of Materials Science, Fudan University, Shanghai, 200438, P. R. China.

*E-mail: jiezhu@glut.edu.cn (J. Zhu); jinlin_1982@126.com (L. Jin); rbwu@fudan.edu.cn (R. Wu)

Materials characterizations

The powder XRD experiments were conducted on Bruker D8, and the source was a Cu-K α radiation ($\lambda = 1.54056 \text{ \AA}$) at 40 kV and 40 mA. SEM measurements were performed on Hitachi S-4800 operated at 2 kV. The TEM, HRTEM, HAADF-STEM, and EDX mapping images were acquired using JEOL JEM-2100F field emission electron microscope operating at 200 kV. XPS measurements were carried out on a Thermo ESCALAB 250Xi spectroscope (Perkin-Elmer) using Al-K α x-rays as the excitation source. Raman spectra of samples were recorded using the confocal Raman spectrometer (LabRAM Aramis) equipped with an excitation laser wavelength of 532 nm. The FT-IR spectra were collected on a Bruker VECTOR 22 spectrometer with KBr disk method. The CAs of droplets on the sample surfaces were recorded by a contact angle measuring device (MDTC-EQ-M07-01, Japan). Zeta potential test was performed by Zetasizer NanoZS90 device. XAS measurements were performed at Beamlines 1W1B at Beijing Synchrotron Radiation Facility (BSRF).

Electrochemical measurements

Preparation of electrocatalyst ink

The working electrode was prepared by dispersing 5 mg of catalyst powder into 1 mL of a mixed solution containing 900 μL ethanol and 100 μL Nafion solution (5 wt%), and followed by ultrasonication for 30 min to obtain uniform slurry. Subsequently, 200 μL of slurry was loaded on a Ni foam (1 cm \times 1 cm) and dried naturally at room temperature.

HER/OER measurements

The hydrogen evolution reaction (HER) and oxygen evolution reaction (OER) performances were evaluated in a standard three-electrode configuration in 1 M KOH using a CHI 760E electrochemical workstation (CH instrument, Chenhua). Wherein a graphite rod electrode and Hg/HgO (KOH saturated) electrode were used as the counter electrode and the reference electrode, respectively. Linear sweep voltammetry (LSV) of HER/OER measurements were taken at a scan rate of 5 mV s $^{-1}$ in N $_2$ - saturated 1 M KOH solution. The potentials measured were referenced to a reversible hydrogen electrode (RHE) according to the Nernst equation: $E(\text{RHE}) = E(\text{Hg}/\text{HgO}) + (0.098 + 0.059\text{pH}) \text{ V}$, and all current densities were normalized to the geometrical surface area. The Tafel slope was obtained from the corresponding LSV curves according to Tafel equation: $\eta = b \cdot \log(j/j_0)$. (η is the overpotential, b is Tafel slope, j is the current density, and j_0 is the exchange current density). Electrochemical surface area (ECSA) was determined by the tested electrochemical double-layer capacitance (C_{dl}) obtained from cyclic voltammogram (CV) measurement. Cyclic voltammograms (CVs) were tested from -0.036 to -0.024 V for HER, and 1.224 to 1.274 V for OER with scan rates ranging from 20 to 100 mV s $^{-1}$. Electrochemical impedance spectroscopy (EIS) tests were carried out from 500,000 to 1 Hz with the amplitude of 5 mV. All the data presented were not corrected for iR losses. The long-term stability was evaluated by chronoamperometric test in 1 M KOH solution.

AEMWE measurements

For AEMWE measurements, nickel foam was preprocessed by HCl, water, and ethanol in turn so as to eliminate the oxides and impurities. Then, the catalysts were dropped onto nickel foam substrate with loading of 1 mg cm $^{-2}$ and used as both the anode and cathode to assemble a two-electrode water electrolysis cell. The polarization curve was recorded in 1 M KOH at a scan rate of 5 mV s $^{-1}$. The stability was evaluated by chronopotentiometric test at 200 mA cm $^{-2}$.

Calculation details

The Vienna Ab Initio Package (VASP) was employed to perform all the density functional theory (DFT) calculations within the generalized gradient approximation (GGA) using the Perdew, Burke, and Enzerhof (PBE) formulation.¹⁻³ The projected augmented wave (PAW) potentials were applied to describe the ionic cores and take valence electrons into account using a plane wave basis set with a kinetic energy cutoff of 450 eV.^{4,5} Partial occupancies of the Kohn-Sham orbitals were allowed using the Gaussian smearing method and a width of 0.05 eV. The electronic energy was considered self-consistent when the energy change was smaller than 10 $^{-5}$ eV. A geometry optimization was considered convergent when the force change was smaller than 0.05 eV/ \AA . Grimme's DFT-D3 methodology was used to describe the dispersion interactions.⁶ The vacuum spacing perpendicular to the plane of the structure is 20 \AA . The Brillouin zone integral utilized the surfaces structures of 2 \times 2 \times 1 monkhorst pack K-point sampling. Finally, the adsorption energies (E_{ads}) were calculated as $E_{\text{ads}} = E_{\text{ad/sub}} - E_{\text{ad}} - E_{\text{sub}}$, where

$E_{\text{ad/sub}}$, E_{ad} and E_{sub} are the total energies of the optimized adsorbate/substrate system, the adsorbate in the structure, and the clean substrate, respectively. The free energy was calculated using the equation:

$$G = E_{\text{ads}} + \text{ZPE} - \text{TS}$$

where G , E_{ads} , ZPE and TS are the free energy, total energy from DFT calculations, zero point energy and entropic contributions, respectively.

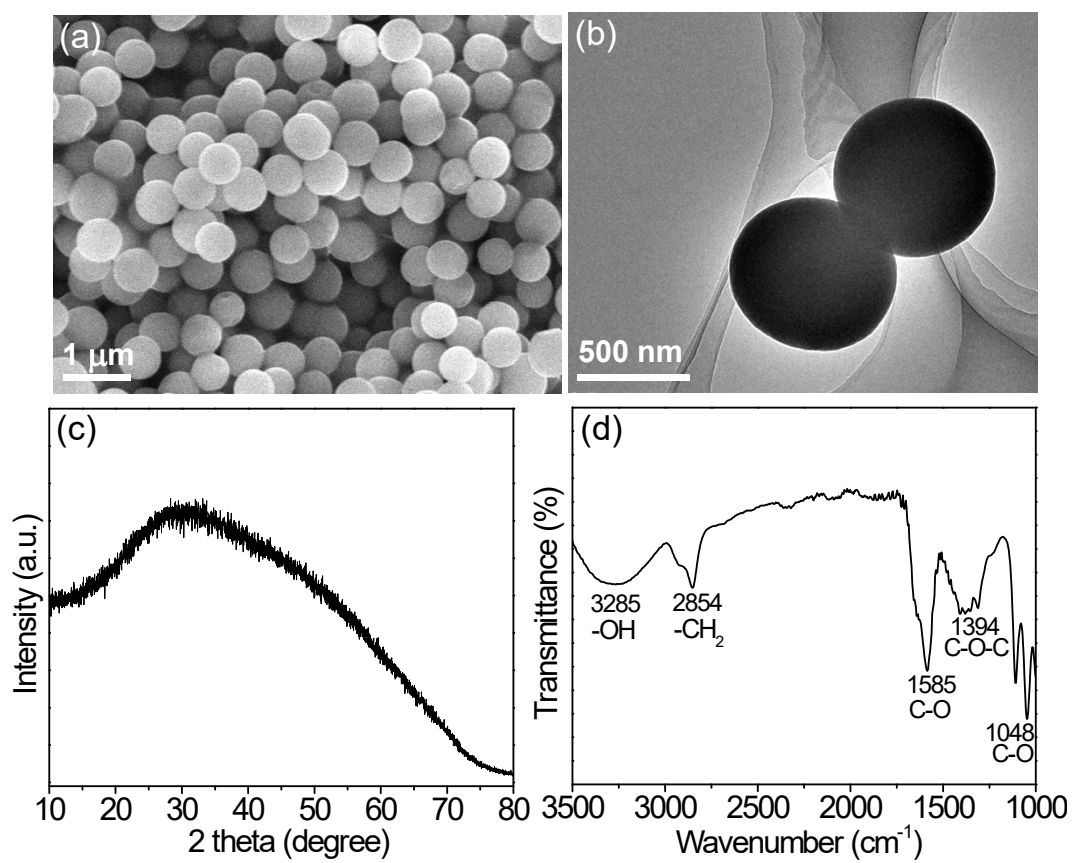


Fig. S1 (a) FE-SEM, (b) TEM, (c) XRD pattern and (d) FTIR spectrum of the Mo-Co-alkoxide precursor.

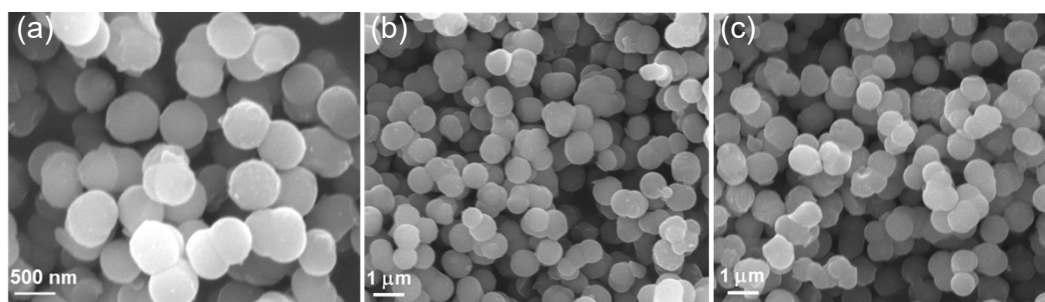


Fig. S2 FE-SEM images of (a) MCS-1, (b) MCS-2 and (c) MCS-0.5.

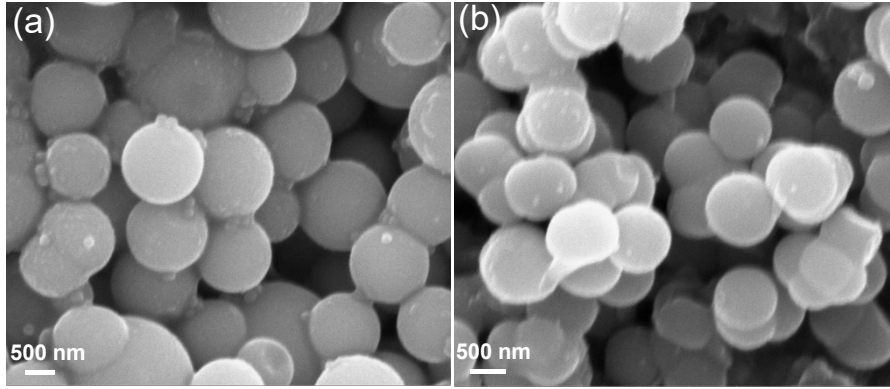


Fig. S3 FE-SEM images of (a) MoS₂ and (b) CoS.

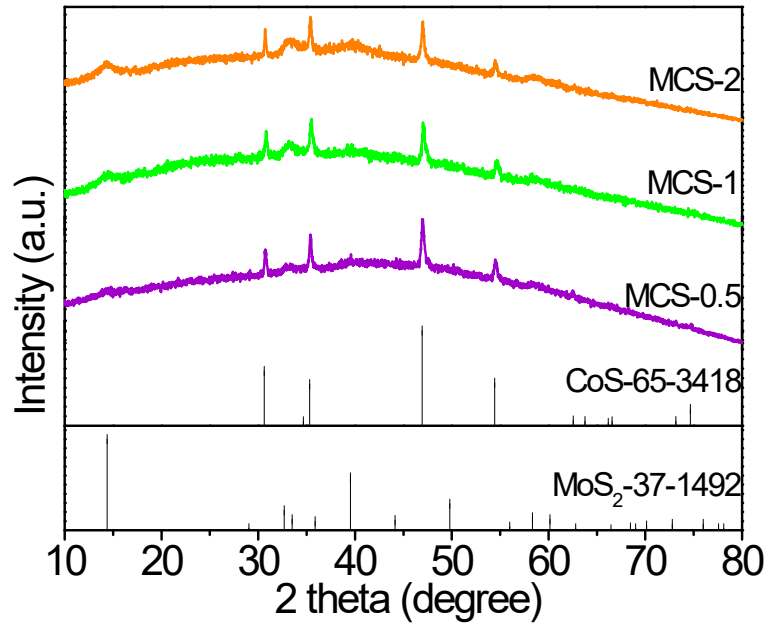


Fig. S4 The XRD pattern of MCS-1, MCS-2 and MCS-0.5 samples.

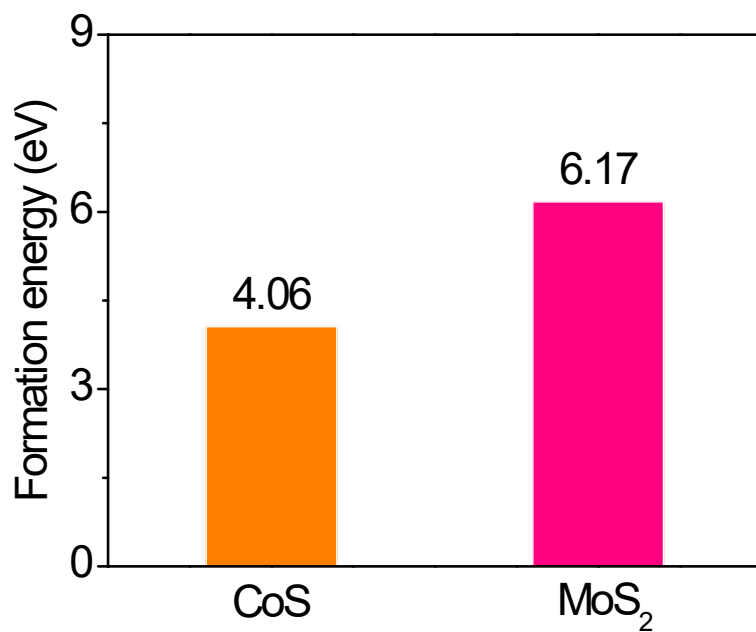


Fig. S5 The formation energies of CoS and MoS₂.

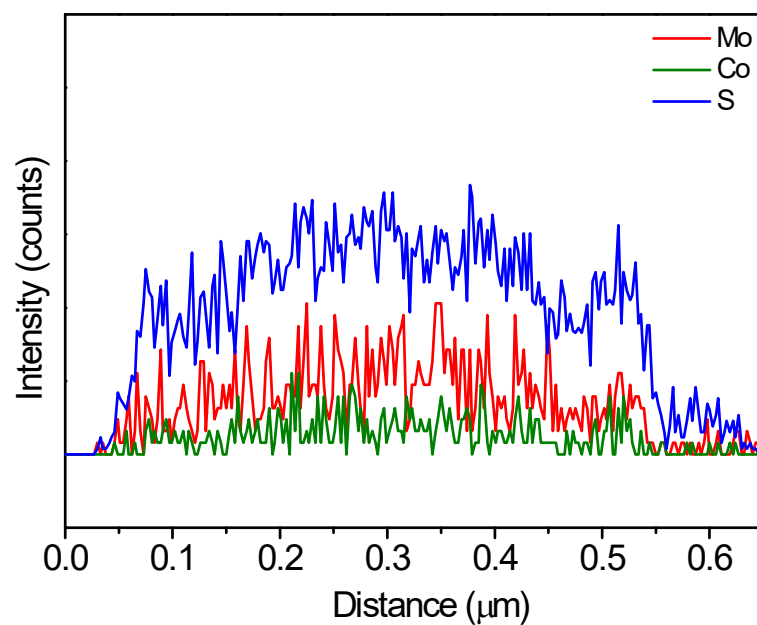


Fig. S6 The EDS line-scanning profile of MCS-1.

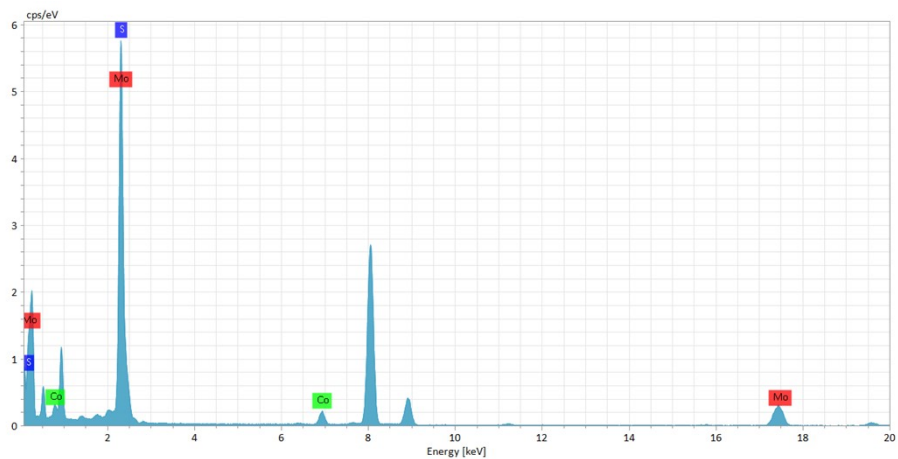


Fig. S7 TEM EDS spectrum of MCS-1.

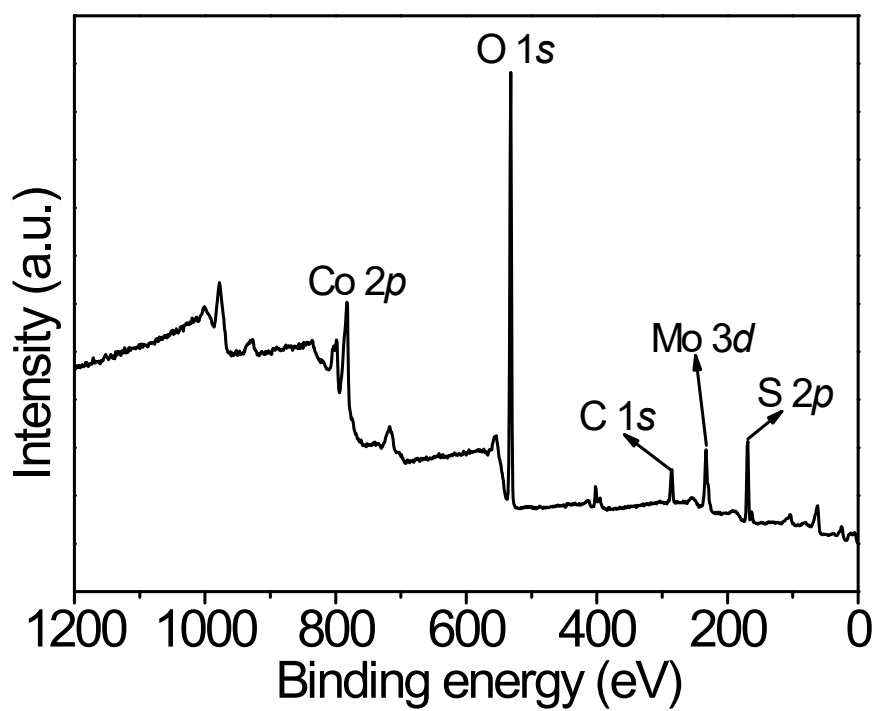


Fig. S8 XPS survey spectrum of MCS-1.

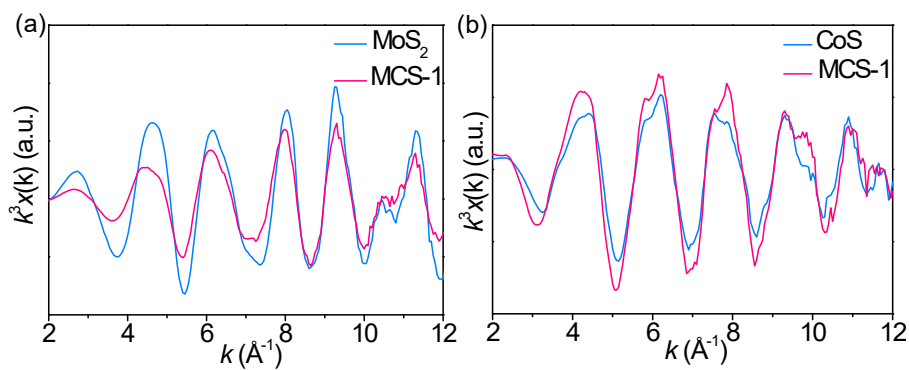


Fig. S9 (a) Mo K-edge $k^3 x(k)$ oscillation curves for MCS-1 and MoS_2 . (b) Co K-edge $k^3 x(k)$ oscillation curves for MCS-1 and CoS.

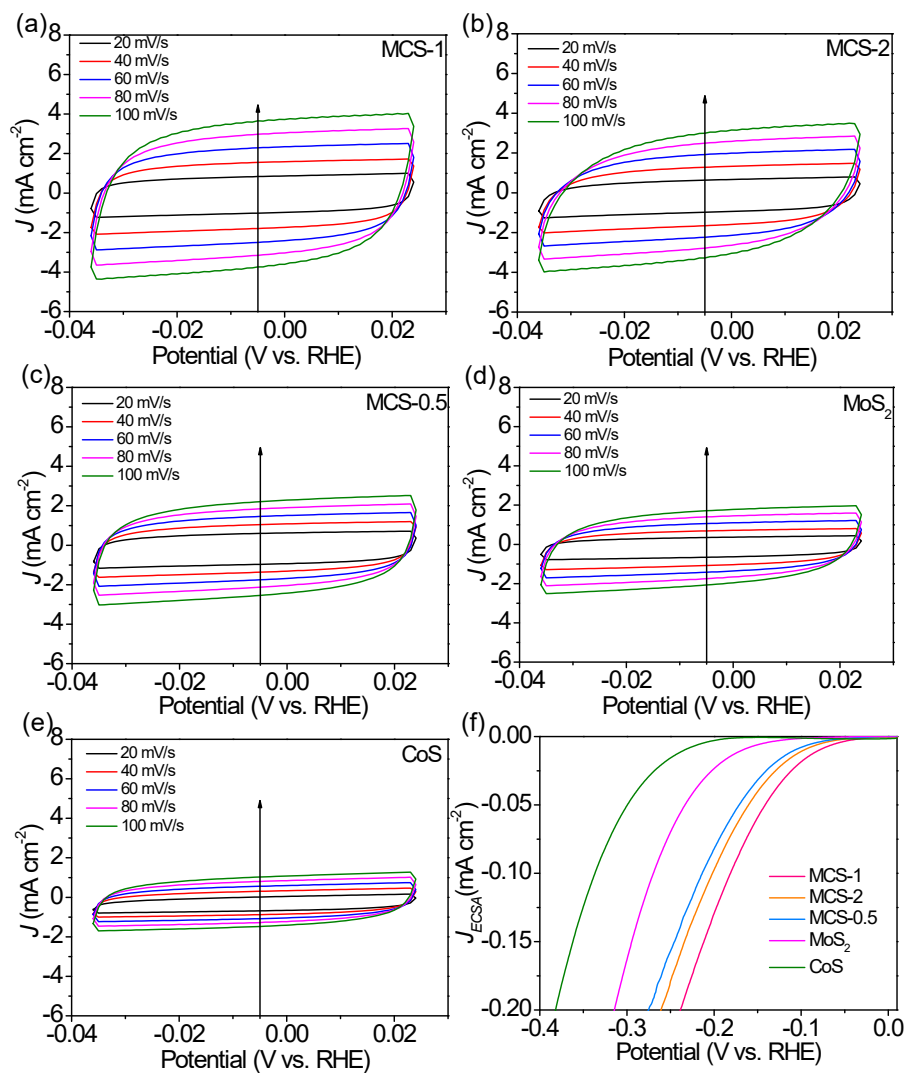


Fig. S10 CV curves of (a) MCS-1, (b) MCS-2, (c) MCS-0.5, (d) MoS_2 and (e) CoS at scan rates of 20-100 mV s^{-1} . (f) ECSA normalized HER polarization curves of MCS-1, MCS-2, MCS-0.5, MoS_2 and CoS.

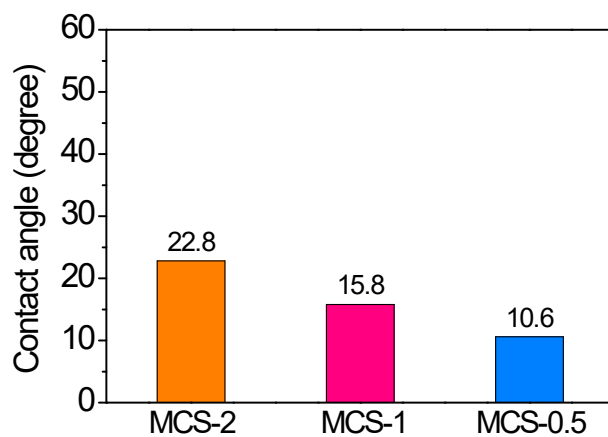


Fig. S11 The contact angles of MCS-1, MCS-2 and MCS-0.5.

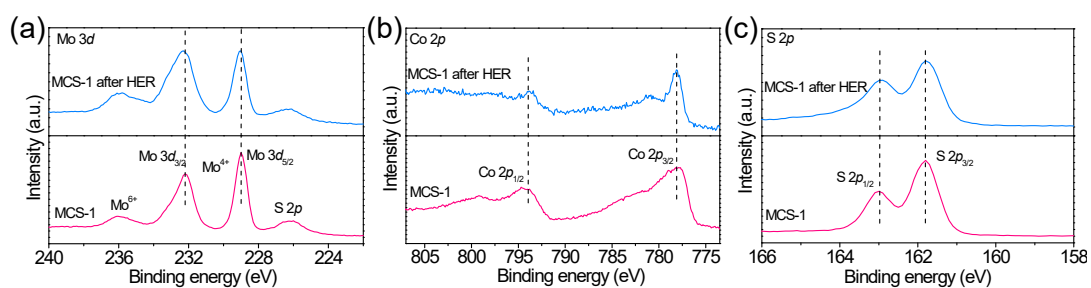


Fig. S12 (a) Mo 3d, (b) Co 2p, (c) S 2p XPS spectra of MCS-1 and MCS-1 after HER stability.

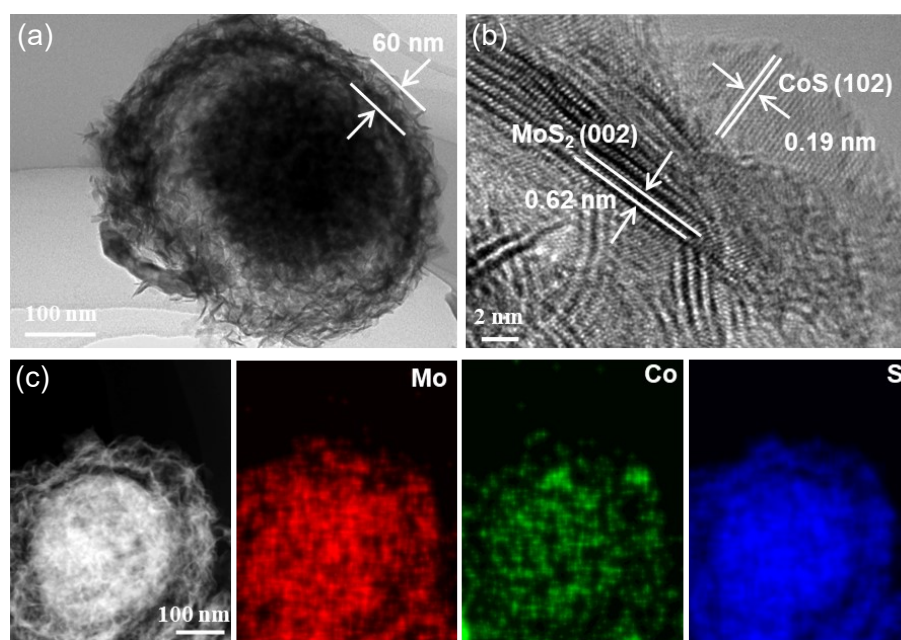


Fig. S13 The (a) TEM, (b) HR-TEM, (c) HAADF-STEM images and the corresponding EDX mappings of MCS-1 after HER stability.

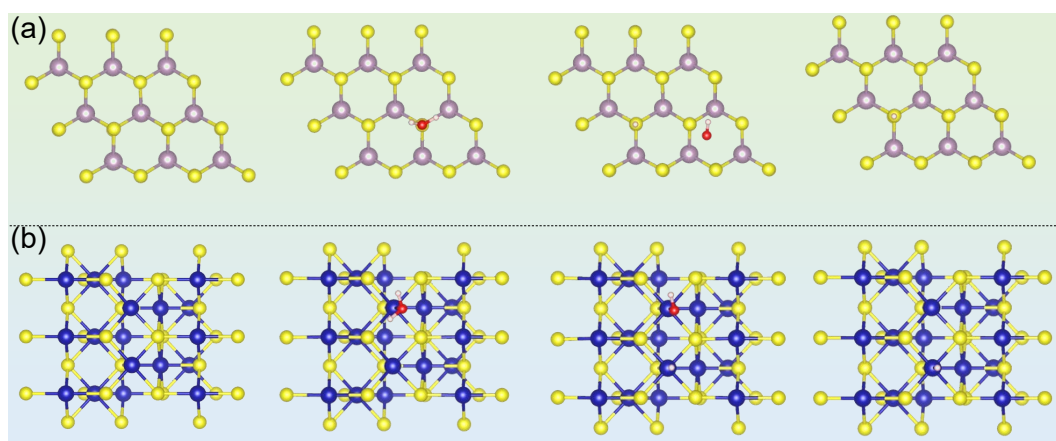


Fig. S14 Optimized adsorption models of each step on the (a) MoS₂ and (b) CoS surface. (Color codes: purple–Mo, yellow–S, blue–Co).

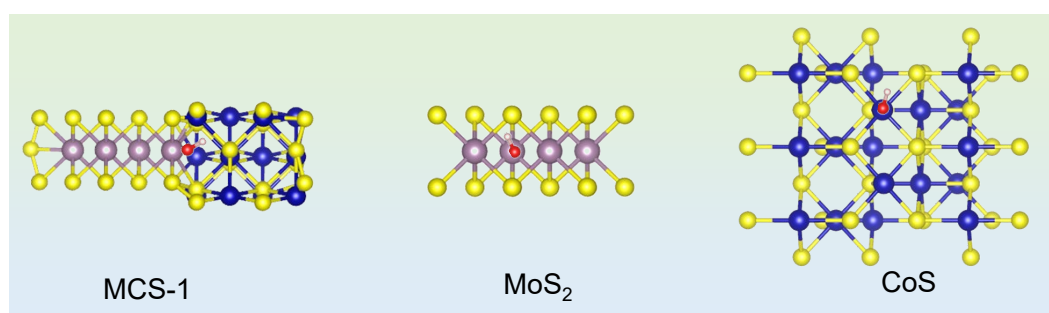


Fig. S15 *OH adsorption configurations on the MCS-1, MoS₂ and CoS surface. (Color codes: purple–Mo, yellow–S, blue–Co).

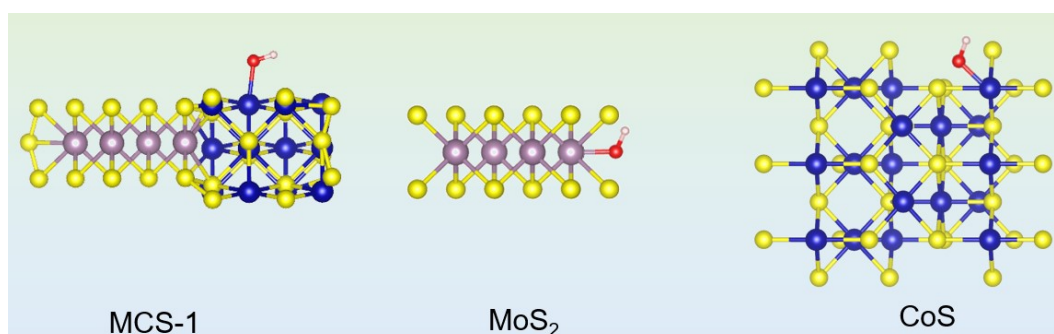


Fig. S16 OH⁻ adsorption configurations on MCS-1, MoS₂ and CoS surface (Color codes: purple–Mo, yellow–S, blue–Co).

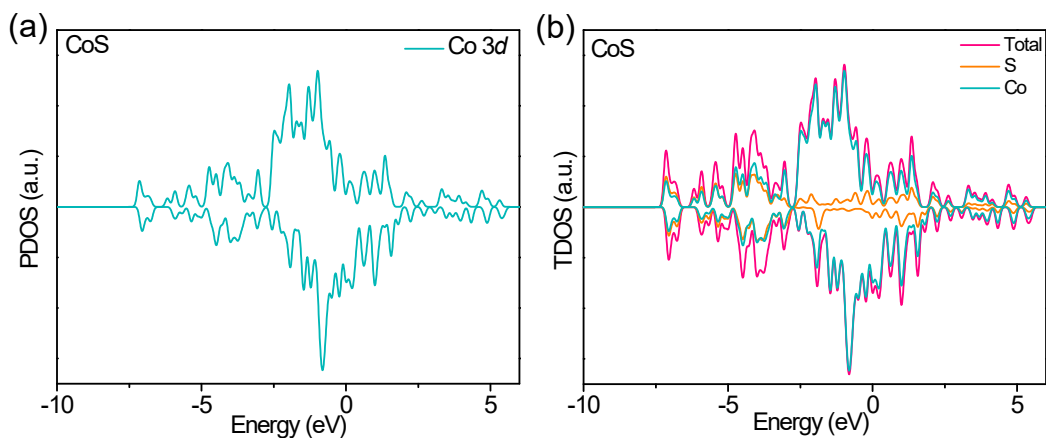


Fig. S17 Calculated (a) PDOSs of Co 3d and (b) TDOSs for CoS.

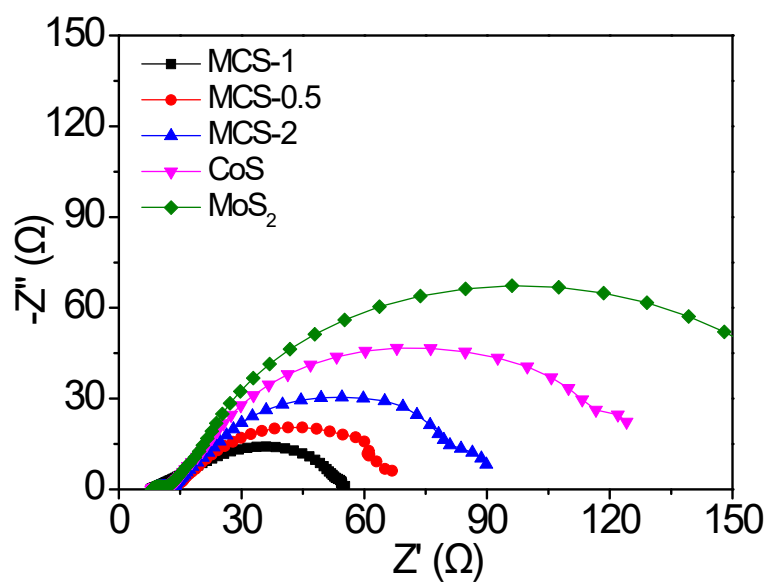


Fig. S18 EIS plots of different samples for OER.

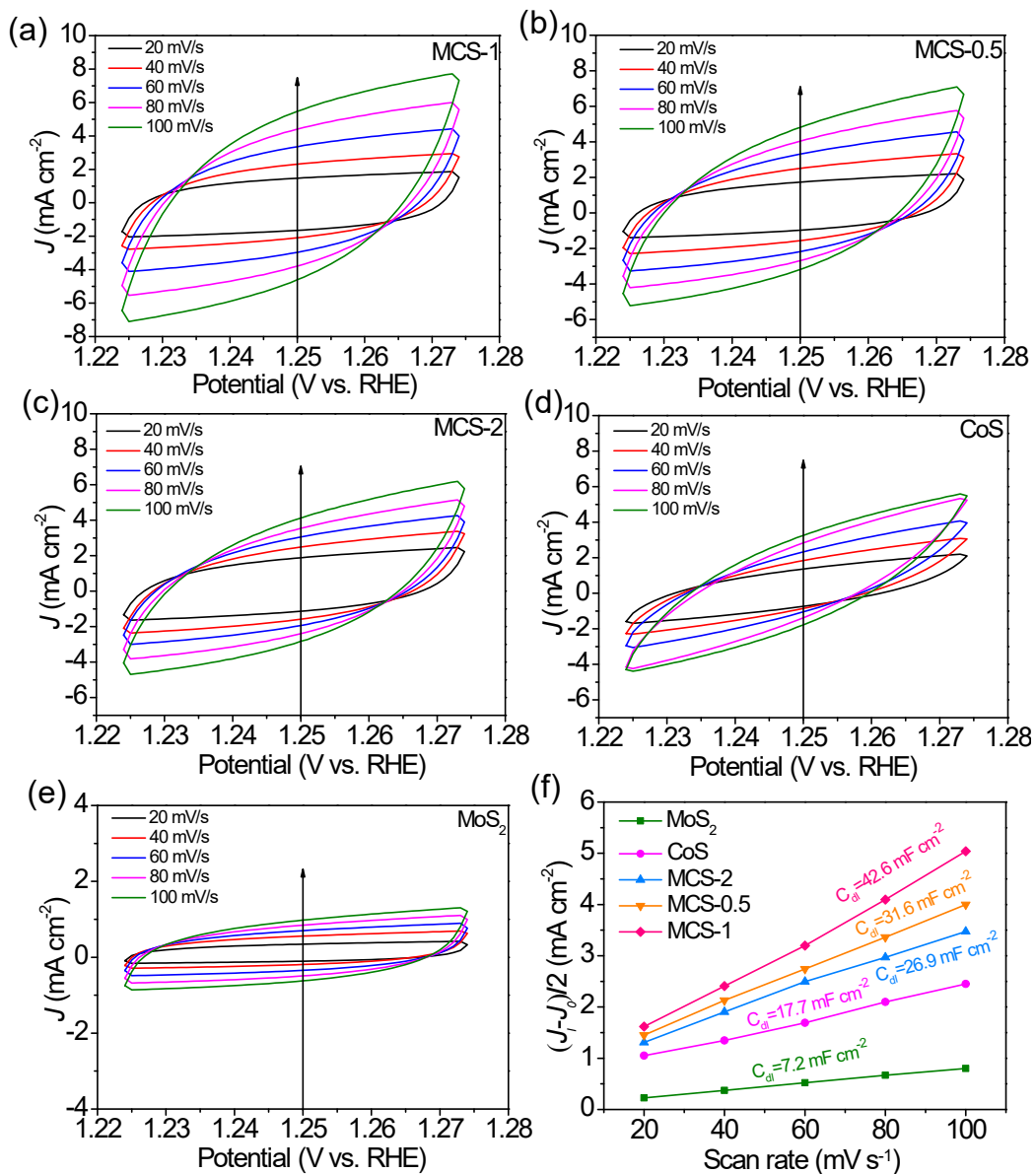


Fig. S19 CV curves of (a) MCS-1, (b) MCS-0.5, (c) MCS-2, (d) CoS and (e) MoS₂ for OER at scan rates of 20-100 mV s⁻¹. (f)

C_{dl} values of MCS-1, MCS-2, MCS-0.5, MoS₂ and CoS.

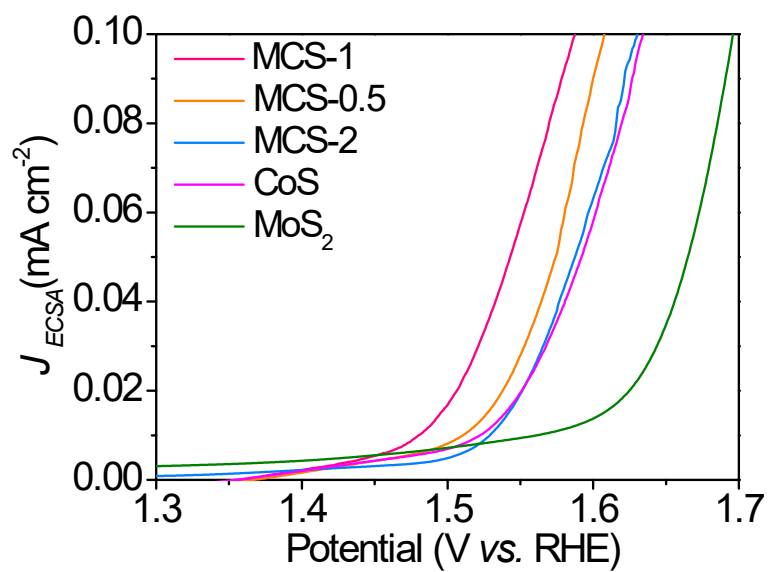


Fig. S20 ECSA normalized OER polarization curves of MCS-1, MCS-0.5, MCS-2, CoS and MoS₂.

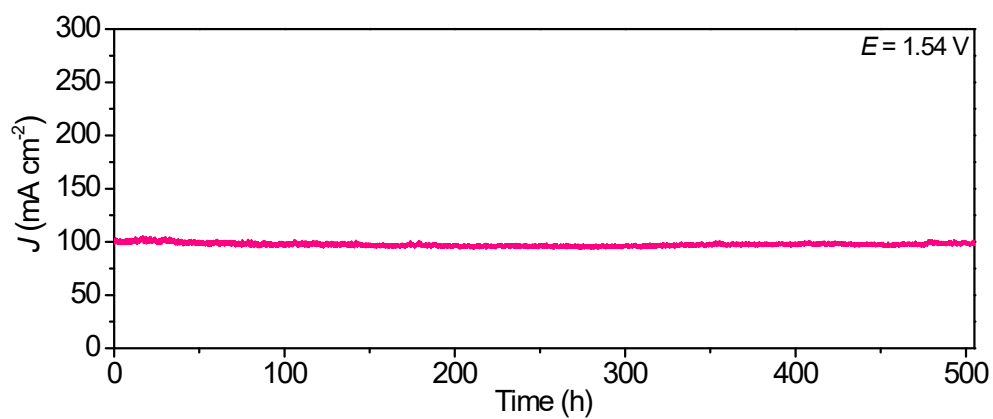


Fig. S21 OER chronoamperometry curves of MCS-1 at the potential of 1.54 V (V vs. RHE).

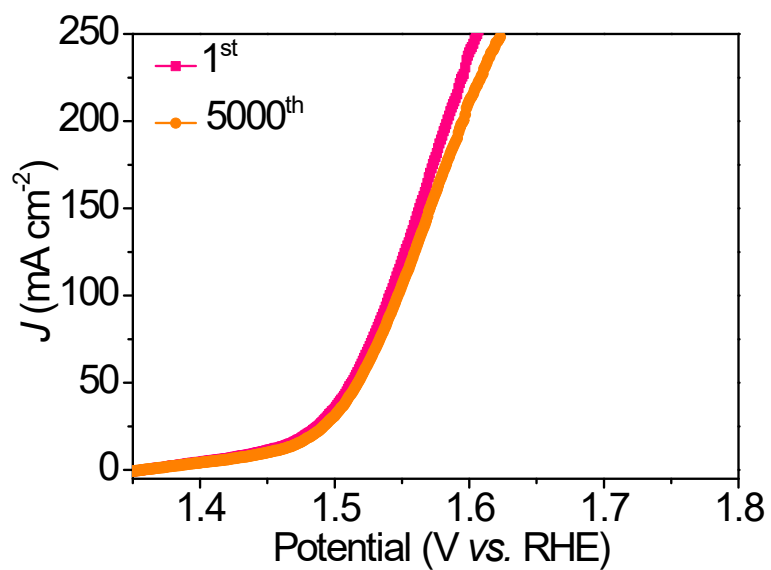


Fig. S22 LSV curves of MCS-1 before and after 5000 cycles for OER.

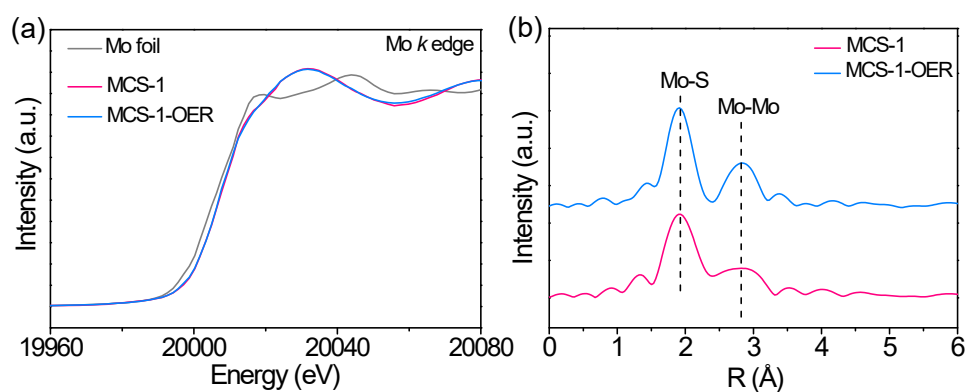


Fig. S23 (a) XANES and (b) EXAFS spectra of MCS-1 before and after OER.

Notes and references

1. G. Kresse and J. Furthmüller, *Phys. Rev. B*, 1996, **54**, 11169–11186.
2. J. P. Perdew, K. Burke and M. Ernzerhof, *Phys. Rev. Lett.*, 1996, **77**, 3865–3868.
3. G. Kresse and D. Joubert, *Phys. Rev. B*, 1999, **59**, 1758–1775.
4. P. E. Blöchl, *Phys. Rev. B*, 1994, **50**, 17953–17979.
5. S. Grimme, J. Antony, S. Ehrlich and H. Krieg, *J. Chem. Phys.*, 2010, **132**, 154104.
6. G. Henkelman, B. P. Uberuaga and H. Jónsson, *J. Chem. Phys.*, 2000, **113**, 9901–9904.